OPEN ACCESS

KING'S College LONDON

King's Research Portal

DOI:
10.1021/acs.langmuir.7b00701

Document Version
Peer reviewed version

Link to publication record in King's Research Portal

Citation for published version (APA):
Puig-Rigall, J., Grillo, I., Dreiss, C. A., & González-Gaitano, G. (2017). Structural and Spectroscopic Characterization of TPGS Micelles: Disruptive Role of Cyclodextrins and Kinetic Pathways. *Langmuir : the ACS journal of surfaces and colloids*, *33*(19), 4737-4747. https://doi.org/10.1021/acs.langmuir.7b00701

Citing this paper
Please note that where the full-text provided on King's Research Portal is the Author Accepted Manuscript or Post-Print version this may differ from the final Published version. If citing, it is advised that you check and use the publisher's definitive version for pagination, volume/issue, and date of publication details. And where the final published version is provided on the Research Portal, if citing you are again advised to check the publisher's website for any subsequent corrections.

General rights
Copyright and moral rights for the publications made accessible in the Research Portal are retained by the authors and/or other copyright owners and it is a condition of accessing publications that users recognize and abide by the legal requirements associated with these rights.

•Users may download and print one copy of any publication from the Research Portal for the purpose of private study or research.
•You may not further distribute the material or use it for any profit-making activity or commercial gain
•You may freely distribute the URL identifying the publication in the Research Portal

Take down policy
If you believe that this document breaches copyright please contact librarypure@kcl.ac.uk providing details, and we will remove access to the work immediately and investigate your claim.

Download date: 05. May. 2023

Structural and spectroscopic characterization of TPGS micelles: disruptive role of cyclodextrins and kinetic pathways

Joan Puig-Rigall[a], *Isabelle Grillo*[b], *Cécile A. Dreiss**[c], *Gustavo González-Gaitano**[a]

[a] Departamento de Química, Universidad de Navarra, 31080 Pamplona, Spain
[b] Institut Laue-Langevin, 71 avenue des Martyrs, B.P. 156, 38042 Grenoble Cedex, France
[c] Institute of Pharmaceutical Science, King's College London, Franklin-Wilkins Building, 150 Stamford Street, London SE1 9NH, UK

Corresponding authors: gaitano@unav.es, cecile.dreiss@kcl.ac.uk

ABSTRACT

The aggregation and structure of D-α-tocopheryl polyethylene glycol succinate micelles, TPGS-1000, an amphiphilic derivative of vitamin E, were characterized by scattering and spectroscopic methods, and the impact of different cyclodextrins (CDs) on the self-assembly studied, with the view of combining these two versatile pharmaceutical excipients in drug formulations. Combined SANS, DLS, time-resolved and steady-state fluorescence emission experiments revealed a core-shell architecture with a high aggregation number (N_{agg} ~ 100) and a highly hydrated PEO corona (~ 11 molecules of solvent per EO unit). Micelles form gradually, with no sharp onset. Structural parameters and hydration of the aggregates were surprisingly stable with both temperature and concentration, a critical advantage for their use in pharmaceutical formulations. CDs were shown to affect the self-assembly of TPGS in different ways. While native CDs induced the precipitation of a solid complex (or pseudopolyrotaxane), methylated β-CDs (in which OH groups on the repeated glucose units are substituted by methoxy groups) led to different outcomes: constructive (micellar expansion), destructive (micellar rupture) or no effect, depending on the number of substituents and whether the substitution pattern was regular or random on the rims of the macrocycle. Time-resolved SANS studies on mixtures of TPGS with regularly dimethylated β-CD (DIMEB), which ruptures the micelles, revealed an almost instantaneous de-micellisation process (< 100 ms), and

showed that the process involved the formation of large aggregates, whose size evolved over time. Micellar rupture is caused by the formation of a TPGS-DIMEB inclusion complex, involving the incorporation of up to three macrocycles on the tocopherol, as shown by 1H and ROESY NMR. Analysis of NMR data using Hill's equation revealed that complex formation is rather cooperative, the threading of a CD favoring the subsequent inclusion of additional CDs on the aliphatic moiety.

INTRODUCTION

D-α-tocopheryl polyethylene glycol succinate, TPGS, is a water soluble derivative of the natural form of vitamin E, produced by the esterification of the crystalline D-α-tocopheryl succinate with polyethylene glycol (SI, Scheme 1). The presence of the PEG chain bestows tocopherol with an amphiphilic character and self-aggregation capability[1], with the known advantages that non-ionic amphiphiles have over cationic and anionic surfactants, in terms of their low sensitivity to electrolytes, good chemical stability and generally better acceptability. TPGS has been extensively investigated for its solubilizing capacity in drug delivery[2–4] and approved by the FDA. Most studies in the literature have used TPGS-1000, which comprises 23 EO units, and a number of drug formulations based on this amphiphile have been developed, including micelles[5,6], microparticles[7], nanoparticles[8] and microemulsifying systems[9], where TPGS is used as a solubilizer, absorption enhancer and a drug-carrier[10,11], especially for poorly water-soluble drugs. Many of these studies have focused on the delivery of anticancer drugs[12], since TPGS inhibits the activity of P-glycoproteins transporters (P-gp), which is responsible for the poor permeability of many cancer drugs through physiological barriers[13]. Its pharmacological response has also been studied and compared to that obtained with other excipients[14,15].

Another class of nano-carriers widely used in pharmaceutical formulations are cyclodextrins (CDs), oligosaccharides formed by the association of several glucopyranose units in a toroid-like arrangement. The three native CDs, α, β and γ-CD, comprise 6, 7 and 8 glucose units in the macrocycle, respectively. The cavity, larger as the number of glucose residues increases, has a relatively hydrophobic character, and is thus capable of lodging a guest molecule, while the outer part of the CD, formed by the primary and secondary hydroxyl groups, is hydrophilic. These hydroxyl groups are susceptible of chemical substitution, improving the properties of native CDs, such as

their solubility or affinity for specific guests. The capacity of trapping molecules in their apolar cavity makes CDs useful in a range of areas, in food as a protectant and to encapsulate flavours and perfumes[16], and in the pharmaceutical industry to solubilize drugs[17–21]. Moving beyond the small hydrophobic molecular guests, interesting supramolecular structures can be formed by the association of cyclodextrins with amphiphilic molecules (surfactants) or larger guests, such as polymers, which open up news prospects for the delivery of active substances[21–24]. For instance, the threading of several cyclodextrins on a polymer chain can offer multi-fold binding, if modified with a suitable ligand[25–27], or be transported within a polyrotaxane structure (by the introduction of suitable stopper-groups) for release at specific sites[28]. The formation of such structures dramatically depends on the type of CD. While native CDs tend to produce solid adducts or precipitates, which have been explored for the production of injectable gels[29], modified CDs tend to form soluble pseudopolyrotaxanes[30,31]. The use of these supramolecular structures for gene and drug delivery has been recently reviewed[32]. The combined use of CDs or their complexes with surfactants in a multifunctional approach requires the compatibility of all compounds involved in the complex. For pharmaceutical formulations in particular, the presence of non-controlled interactions or competition between the different components, could dramatically affect the efficacy of drug encapsulation and drug delivery, hence the necessity to carefully characterise structures and interactions in cyclodextrin-based multi-compartmented delivery systems.

Within this framework, this investigation has two objectives. In the first step, we fully characterize the aggregation behavior of TPGS 1000 and its micellar structures, through the combined use of spectroscopic (UV-visible, fluorescence and NMR) and scattering techniques (SANS and DLS). In a second step, we explore the impact of both native and substituted cyclodextrins on the self-association of TPGS to assess the combined use of these excipients as drug carriers, a topic that has not been addressed yet in the literature. We have focused in particular on the dimethylated derivative of βCD, heptakis(2,6-di-O-methyl)-β-cyclodextrin (DIMEB), which is known to have an important disaggregating impact on non-ionic[30,33] surfactants and, due to its well-defined rim substitution, enables a detailed structural characterization of the complexes formed, thus helping understand the behavior of other substituted CDs.

MATERIALS AND METHODS

Materials. Native cyclodextrins: α-cyclodextrin (≥98%); β-cyclodextrin (≥97%); γ-cyclodextrin (≥98%) (with water contents of 10%, 14% and 10%, respectively, as determined by TGA) were obtained from Sigma-Aldrich. Substituted cyclodextrins: heptakis(2,6-di-*O*-methyl)-β-cyclodextrin (DIMEB, Sigma, 98%), heptakis(2,3,6-tri-O-methyl)-β-cyclodextrin (TRIMEB, 90%), (2-hydroxyethyl)-β-cyclodextrin (HEBCD, 0.7 molar substitution), (2-hydroxypropyl)-β-cyclodextrin (HPBCD, 0.8 molar substitution), (2-hydroxypropyl)-γ-cyclodextrin (HPGCD, 0.6 molar substitution), and randomly methylated β-cyclodextrin (RAMEB, 1.6−2.0 moles of CH_3 per glucose unit) were all obtained from Sigma-Aldrich. The repeating units of each CD are available as Supporting Information (Scheme 2). D-α-tocopheryl polyethylene glycol succinate (TPGS) was a gift from Antares Health Products Inc, with a PEG molecular weight of 1000 (23 EO units). All the concentrations are expressed in weight percentage, unless otherwise stated.

Electronic molecular absorption and emission studies. UV-Vis absorption spectra were recorded on an 8453 UV-Vis Diode Array System spectrophotometer (200 nm to 800 nm), using 1 cm path-length quartz cuvettes. Emission spectra and fluorescence lifetimes were measured with a FLS920 spectrofluorimeter (Edinburgh Instruments), in 1 cm path-length quartz cuvettes. A 500 W xenon lamp was used as the source for the steady state fluorescence experiments, while for the time resolved experiments the source was switched to a 300 nm pulsed diode, triggered with a PDL 800-D pulse generator (PicoQuant). Data collection was stopped after 1000 counts on the detector to build the fluorescence decay curves. Curve fitting to obtain the fluorescence lifetimes was performed with FAST software (Edinburgh Instruments Ltd.), by deconvolution with the scattering decay of a diluted Ludox® solution.

NMR spectroscopy. A Bruker Advance 400 MHz spectrometer was used for recording all the monodimensional 1H-NMR and 1H-COSY spectra. 2D-ROESY experiments were performed with a Bruker AVIII 700, at 700 MHz. Deuterated solvents used were DMSO (deuterium content > 99%), for signal assignation of TPGS and analysis of the compositions of the solid complexes, and D_2O (≥99.85% in deuterated component) for the 1D and 2D studies of the complexes with DIMEB.

Small-Angle Neutron Scattering (SANS). Static small-angle neutron scattering (SANS) experiments were carried out on LOQ instrument at ISIS spallation neutron source (ISIS, Rutherford-Appleton Laboratory, STFC, Didcot, Oxford). LOQ uses incident wavelengths from 2.2 to 10.0 Å, sorted by time-of-flight, with a fixed sample-detector

distance of 4.1 m, which provides a range of scattering vectors, *q*, from 0.009 to 0.29 Å^{-1}. The samples were prepared in D_2O (Aldrich, > 99.9% in D) and placed in clean disc-shaped quartz cells (Hellma) of either 1 or 2 mm path length, controlling the temperature with an external thermostat. All scattering data were first normalized for sample transmission and then background-corrected using a quartz cell filled with D_2O to compensate for inherent instrumental background, and finally corrected for linearity and efficiency of the detector response using instrument-specific software package. The data were then converted to differential scattering cross-sections expressed in absolute units of cm^{-1} using standard procedures at ISIS.

SANS data analysis was performed with SasView 3.1.0 software[34]. Scattering curves from the micelles were fitted to a core-shell sphere (CSS) model combined with a hard-sphere (HS) structure factor. In the data analysis, the polydispersity was left free, as well as the scattering length density (sld) of the core and shell. The number of water molecules in the hydrophilic corona can be estimated from the fitted value of the sld of the shell, ρ_{shell} (a weighted average between the sld of pure PEO and D_2O), and micellar dimensions returned by the fits. The volume fraction of solvent in the corona, x_{solv} is related to ρ_{shell}, ρ_{EO} and ρ_{D_2O} by:

$$x_{solv} = \frac{\rho_{shell} - \rho_{EO}}{\rho_{D_2O} - \rho_{EO}} \qquad \text{Eq. 1}$$

The number of water molecules, n_{solv}, in the shell is calculated from:

$$n_{solv} = x_{solv} \frac{v_{shell}}{v_{D_2O}} \qquad \text{Eq. 2}$$

where v_{D_2O} is the volume of a molecule of solvent. The number of water molecules per EO group, n_{solv}/EO, can then be calculated from Eq. 2 and the aggregation number, N_{agg}, obtained from the hydration of the shell and the structural parameters of the core-shell model. Provided that the amount of water inside the core is negligible, the volume of the micelle is:

$$v_m = N_{agg} v_s + x_{solv} v_{shell} \qquad \text{Eq. 3}$$

where v_s is the volume of a surfactant molecule (462 cm^{3}mol^{-1}, from the manufacturer's specifications). N_{agg} is obtained by introducing into the equation the volume fraction of solvent in the shell, x_{solv}, from Eq. 1.

Time-Resolved SANS (TR-SANS). Kinetic SANS measurements were carried out on D22 at the ILL, combined with a stopped-flow unit, which allows for rapid mixing of several solutions and triggers the reaction with data acquisition, with acquisition times of the order of 100 ms.[35] The wavelength λ was set at 6 Å, the peak flux of the cold source. The sample-to-detector distance was 4 m, with a collimation at 5.6 m and a detector offset of 400 mm to maximize the available q range ($1.2 \cdot 10^{-2} < q < 0.26$ Å^{-1}). A 7×10 mm^2 sample aperture was used, and the sample path length in the Biologic SFM-300 stopped-flow apparatus was 1 mm and the temperature was set to 40ºC. Raw data were corrected for electronic background and empty cell and normalized by water using the proprietary *Lamp* ILL software (Large Array Manipulation) developed for SANS data treatment[36]. The scattering measurements were made with an acquisition time for each frame n of t_n following a geometric series with

$$t_n = a^{n-1} t_1 \quad \text{and} \quad T_n = \frac{1-a^n}{1-a} t_1 \qquad \text{Eq. 4}$$

T_n is the accumulated time after mixing, with t_1 = 100 ms and a = 1.1. Sixty eight frames were measured for a total time of 653 s, after which 20 additional frames were measured with 6 s of exposure each. The average time after mixing T_{AMn} for the n^{th} run is

$$T_{AM1} = \frac{t_1}{2} + t_{DT} \quad \text{and} \quad T_{AMn} = \frac{T_{n-1}+T_n}{2} \qquad \text{Eq. 5}$$

t_{DT} being the dead time needed to fill the cell, estimated at 70 ms for the flow rate used. The stock solutions of TPGS and CD were prepared by weighing the required amounts of surfactant, DIMEB and deuterated water. Appropriate volumes of stock solutions (total of 250 µL) were then mixed in the stopped-flow cell at a flow rate of 3 mL/s to obtain the target concentrations. Datasets of the experiments can be found on the ILL website[37].

Dynamic light scattering (DLS). Size distributions of TPGS in water and mixtures with substituted CDs were obtained with a photon correlation spectrometer (Malvern Zetasizer Nano) with a laser wavelength of 633 nm. The samples were filtered prior to the measurements by 0.22 µm Millex syringe PVDF filters onto semi-micro glass cells, and the temperature controlled with 0.1˚C accuracy by the built-in Peltier in the cell compartment. The viscosity and refractive index of the solvent at different temperatures were taken into account to obtain the particle size distribution from the analysis of the autocorrelation function, which was performed with the Zetasizer software in the high

resolution mode to better distinguish overlapping distributions. The diffusion coefficients of TPGS as a function of concentration were obtained on a DynaPro-MS/X photon correlation spectrometer (90º optics, 822 nm diode laser). The experiments were performed at 25.0 and 50.0ºC (0.1˚C accuracy). Samples were filtered by 0.02 μm filters (Whatman Anotop). The intensity size distributions were obtained by regularization analysis with Dynamics 6.0 software.

RESULTS AND DISCUSSION

Micellisation process of TPGS

The aromatic moiety of tocopherol accounts for the UV-vis absorption of the molecule, with a maximum at λ = 285 nm. The molar absorptivity at λ_{max}, ε, can be obtained by a linear fit to the Beer-Lambert law, resulting in (1.86 ± 0.04) $\times 10^3$ $M^{-1}cm^{-1}$ (SI, Figure S1). The low molar absorptivity of TPGS prevents a reliable estimation of the cmc by this technique, which can be overcome by using the emission fluorescence. Figure 1A shows TPGS emission spectra from 295 nm to 440 nm at λ_{ex} = 285 nm over a range of concentrations up to 0.04%. At this excitation wavelength, Raman scattering due to OH stretching bands from the solvent partially overlaps with the fluorescence, and was thus subtracted from the spectra. The fluorescence intensity at λ_{max} = 314 nm against concentration increases smoothly (Figure 1B), with no sharp change of slope marking the onset of aggregation. As an approximation, if aggregation modes such as fusion of small micelles is discarded, the micellization can be described by the equilibrium $NS \Leftrightarrow S_N$, where S is the surfactant and S_N the micelles of aggregation number N. The concentration of free surfactant and micelles is related to the thermodynamic constant through the mass action law: $K = [S_N]/\,[S]^N$. The presence of a power N makes it convenient to represent TPGS concentration on a log scale, as shown in Figure 1B. The inflexion point then corresponds to the concentration at which the change in fluorescence is steepest and can be taken as a critical concentration. A sigmoidal fit to the plot gives a cmc of 0.020 ± 0.005 %, obtained from three replicates, in good agreement with literature results obtained with pyrene fluorescence[1,4].

Further insight into the micellisation process is obtained from fluorescence lifetime spectroscopy. If there are different emitting species, the fluorescence decay upon an excitation pulse is given by:

$$I_F(t) = A + \sum B_i \mathrm{e}^{-\mathrm{t}/\tau_i} \qquad \text{Eq. 6}$$

where B_i is an amplitude factor related to the intrinsic quantum yield of fluorescence and concentration of the *i* species, τ_i its fluorescence lifetime and *A* the background. Two exponentials were used to fit the data (SI, Table T1). The fluorescence lifetime of vitamin E has been reported[38] as 0.5 ns, therefore the fast decay corresponds to the monomeric form, while the second contribution, at ca. 2.2 ns, is ascribed to the micellised surfactant. The micellar fraction can be deduced from the ratio of the pre-exponential factors, F_{mic}/F_T (SI, Table T1); its value increases steadily over time, without a clear break-point, confirming the gradual formation of micelles rather than their sudden onset.

TPGS micellar structure

Dynamic Light Scattering (DLS) measurements of a 1% TPGS solution (well above the cmc) show a monomodal, narrow size distribution, corresponding to a radius of about 5 nm (Figure 2A). The diffusion coefficient, *D*, as a function of the concentration was measured at two temperatures (SI, Figure S2). The intercept of a linear fit to the experimental data gives the diffusion coefficient at infinite dilution (D_0), from which the hydrodynamic radius, R_h^0, of the micelles can be deduced from the Stokes-Einstein equation for spheres:

$$R_h^0 = \frac{\mathrm{k_B T}}{6\pi\eta \mathrm{D_0}} \qquad \text{Eq. 7}$$

where k_B is the Boltzmann constant, *T* the absolute temperature and η the solvent viscosity at the experimental temperature. The diffusion coefficients at infinite dilution obtained are: $(4.8 \pm 0.2)\times10^{-7}$ cm^2s^{-1} at 25ºC and $(8.4 \pm 0.6)\times10^{-7}$ cm^2s^{-1} at 50ºC, which correspond to an R_h^0 of 5.1 nm and 5.0 nm, respectively, showing negligible sensitivity to temperature, while the weak slope suggests a constant size over a wide range of concentrations. From these values, a rough estimation of the aggregation number (N_{agg}) is obtained by dividing the volume of a sphere of radius R_h^0 by the molar volume of the monomer. With a density of 1.06 g cm^{-3} for TPGS (value at 45ºC, from the manufacturer), N_{agg} is ca. 200, a value most likely overestimated since the corona must be largely hydrated.

SANS measurements were carried out to achieve a more detailed description of the micelles. As an example, Figure 2 shows the scattering of a 1% TPGS solution in D_2O at 20ºC. Fits of the data to a CSS-HS model converge towards small ρ_{core} values, of the order of 1×10^{-7} Å^{-2}, indicating a rather dehydrated core. The resulting polydispersities were of the order 0.15-0.2, in agreement with the values obtained by DLS. The hydration of the shell and the aggregation number, N_{agg}, were obtained from the dimensions of the micelle and fitted sld of the shell (cf Experimental Section).

Table 1. Structural parameters of TPGS micelles extracted from SANS data analysis: R_c (core radius), t (shell thickness), ϕ (volume fraction), ρ_{shell} (scattering length density of the shell), N_{agg} (aggregation number), $n_{sol/EO}$ (number of solvent molecules per EO unit in the shell).

	R_c / Å	t / Å	ϕ	$\rho_{shell} \times 10^6$ / Å^{-2}	N_{agg}	n_{sol}/ EO
1%, 20ºC	37.7± 0.9	26 ± 2	0.029	6.19 ± 0.09	105	11.5
1%, 40ºC	37.7± 0.8	25 ± 2	0.027	6.13 ± 0.09	109	10.6
5%, 20ºC	37.0 ± 0.2	26.5 ± 0.2	0.131	6.09 ± 0.02	106	11.2
5%, 40ºC	37.5 ± 0.2	23.9 ± 0.2	0.115	6.09 ± 0.02	108	9.6

TPGS have an overall radius of ca. 63 Å, about 10 Å larger than the hydrodynamic radius obtained from DLS extrapolated to zero concentration (Figure 2). Temperature has a limited effect on micellar structure (Table 1). The hydration of the shell (10-12 solvent molecules per EO unit, equivalent to 96% of D_2O in volume) suggests an extensively hydrated shell, which slightly reduces with temperature, accompanied by a slight shrinking of the shell. This high solvent penetration is usual with non-ionic surfactants based on EO units; [30,31,39] for instance, X-shaped PEO-PPO block copolymer Tetronic 904, with 15 EOs per arm, has 6-12 solvent molecules per EO unit in the shell[30]. The relatively high aggregation numbers suggest that the tocopherol moieties are closely packed in the micellar core. However, the core radius, R_c, at ca. 37 Å, is slightly larger than the length of a fully extended tocopherol-succinate molecule (ca. 30 Å), thus suggesting the absence of interdigitation of the hydrophobic tails. The N_{agg} reported here are substantially higher than the value of 10 reported by Sadoqi et al.[1] measured by the static quenching of pyrene fluorescence with N,N-dibutylaniline DBA, a value that seems quite low considering the size of the

micelles and the high hydrophobicity of the tocopherol moiety. As for the effect of concentration, micelles at 1% or 5% have virtually the same aggregation number, size, and number of solvent molecules per EO in the shell. Overall, it can be concluded that the structure of TPGS micelles is very stable with both concentration and temperature, an interesting point to consider for applications of TPGS as a drug carrier. In the next section we turn to the effect of cyclodextrins on the self-assembly structures of TPGS.

Effect of cyclodextrins on TPGS aggregation

The addition of native cyclodextrins, α, β or γCD, well below their solubility limit, to a 1% TPGS solution leads to the formation of, first, turbid solutions, then white precipitates. In the case of 1% αCD, the haziness is less pronounced, and DLS analysis reveals a size distribution similar to TPGS micelles (ca. 5 nm), together with a large distribution at the nominal diameter of the filter pore used (0.2 μm), most likely due to the self-aggregation which is known to occur in native CDs[40] (SI, Figure S3). The precipitates originate from pseudopolyrotaxane formation by threading of the CDs on the PEO blocks of the surfactant and further stabilization by hydrogen bonding between adjacent CD[41]. The binding of CDs to polymers based on EO units is rather selective, αCD being the macrocycle with most affinity to PEO[42]. The yield of the complexation obtained by weighing the dried precipitate after centrifugation are 35, 47 and 54%, for α, β and γCD, respectively. The CD/TPGS molar ratio in the complexes (analyzed by NMR after redissolution of the precipitates) follow the same trend: 3.8, 5.7 and 6.2 for α, β and γCD, respectively. The fact that αCD produces the lowest yield and CD/TPGS ratio is a consequence of its narrow cavity, which only enables it to thread onto the PEO chain, while the wider β and γCD are expected to also complex with the tocopherol moiety.

Substitution of some or all of the hydroxyl groups on the macrocycles can affect the complexation capability quite dramatically. Modified CDs have been shown in particular to induce a de-micellisation process, either with Pluronics[43–45], Tetronics, or wormlike micelles[46], hence a similar behavior may be expected with TPGS. Figure 2A shows the effect of adding dimethylated β-cyclodextrin (DIMEB) to a dilute TPGS solution at 20ºC from DLS data. At low DIMEB concentration (1%), micelles are still present, but with 5% DIMEB, the micellar peak disappears, while a lower peak (R_h ~ 2 nm) appears, ascribed to the TPGS-DIMEB complex, and large and

polydisperse aggregates (ranging from a few nanometers to almost 100 nm) appear (whose contribution either in mass or volume must be very small). Thus, complete break-up of the micelles takes place above a critical amount of CD. The same scenario is observed at higher temperature (40ºC), with micelles remaining intact at 1% DIMEB and disappearing with 5% DIMEB. The effect of DIMEB at different temperatures is corroborated by SANS analysis (Figure 3). The scattering from the complex was modeled by a simple monodisperse Gaussian coil (Figure 3, solid lines), resulting in a R_g of 12.6 Å (20ºC) and 12.7 Å (40ºC). Both values are in fair agreement with the hydrodynamic radii obtained by DLS of 1.8 and 1.9 nm at both temperatures (Figure 2A), considering $R_g^2 = 3/5\ R_h^2$ for a hydrodynamic sphere. The slight increase of intensity at very low q (Figure 3) suggests the presence of larger size objects, which may result from further association of the complexes.

The nature of the modified groups on the macrocycle, as well as the extent and regularity of the substitution can have a substantial impact on the complexation, as reported before[43,46]. For instance, the permethylated βCD (TRIMEB), which has all three hydroxyl groups substituted rather than two, does not affect TPGS micelles at 5%, either at 20 or 40ºC (data not shown). The case of RAMEB, a randomly methylated CD, produces the exact opposite effect, as it induces the association of TPGS micelles into large and polydisperse aggregates of ca. 28 nm radius. These aggregates increase in size while becoming more monodisperse with temperature (42, 43, and 49 nm in radius, at 30, 40, and 50ºC, respectively) (Figure 2B). This randomly substituted CD has been reported to act as a micelle expander of a poloxamer at high concentrations, a property that was then exploited to produce mesoporous γ-alumina[47]. The authors suggested that RAMEB would be located in the outer shell of the poloxamer micelles, interacting with the PEO segments. A similar effect with TPGS could explain the observed micellar growth, given the identical nature of the hydrophilic corona. Other substituted βCD, hydroxyethyl or -propyl-βCD (HEBCD and HPBCD) do not impact the micelles at 1%, while HPGCD, with a larger cavity, does not have any effect either, at concentrations up to 5% (at either 20ºC or 40ºC).

The above results evidence that not only the nature but also the extent and the regularity of the chemical substituents along the CD rim are paramount in dictating the final outcome of complexation: either destructive (micellar break-up) or constructive (micellar expansion). While native CDs produce solid

pseudopolyrotaxanes, regularly methylated βCD (DIMEB), with a lower capacity of hydrogen-bond formation between adjacent macrocycles, has a strong disruptive effect on TPGS micelles. Instead, thrice-methylated TRIMEB has no detectable effect at the same concentration, while the randomly substituted RAMEB induces micellar association into large aggregates. In the following, we narrow down the focus on DIMEB, since it is the macrocycle with the most drastic effect on TPGS micelles, a factor of importance if we envisage the concomitant use of CD and TPGS in a drug delivery system.

TPGS micellar rupture induced by DIMEB

Changes in the aggregation behavior of TPGS are likely to be reflected by variations in the UV absorbance or fluorescence spectra, arising either from its self-association or the formation of a CD-TPGS inclusion complex. Below the cmc (0.01% TPGS), the addition of 3% DIMEB does not affect λ_{max} (285 nm) in UV absorbance, but slight differences in the shape of the band are observed, which are more noticeable in the fluorescence excitation spectrum (Figure 4A, shown in a normalized scale for comparison purposes). In the fluorescence emission spectrum (Figure 4B) an enhancement of the fluorescence and a blue-shift of λ_{em}, from 314 to 303 nm, are observed. This evidence reflects changes in the micropolarity of the aromatic moiety of tocopherol, due to the presence of the macrocycle.

Fluorescence decays obtained from fluorescence lifetime spectroscopy on the same solutions were fitted with two exponential decays, with lifetimes τ_1 =0.303 ± 0.002 ns and τ_2 = 2.25 ± 0.04 ns and respective contributions of 98% and 2% (SI, Figure S5). τ_1 is slightly lower than the lifetime of TPGS monomers (0.4 ns, SI, Table T1), thus most likely corresponds to the complex with DIMEB, while the second decay τ_2 can be ascribed to micellised TPGS. It is clear that the addition of DIMEB drastically reduces the micellised fraction, compared to TPGS alone (SI, Table T1).

Next, we employed time-resolved SANS (TR-SANS) to investigate the kinetics of de-micellization induced by DIMEB. A stopped-flow device was used to rapidly mix stock solutions of TPGS and DIMEB, achieving a final concentration of 1% surfactant and 3% DIMEB (Figure 5). The first frame is measured ca. 100 ms after mixing, and by this time the micelles have largely disappeared (as inferred by the drop in intensity), while the uprising curve at low q denotes the presence of large

aggregates. The drop in intensity is reminiscent of the micellar break-up obtained with 1% TPGS and 5% DIMEB (Figure 3), while the formation of larger structures is more pronounced at this lower CD concentration of 3%. DLS measurements in D_2O also confirm the presence of these large aggregates, which seem to be critically dependent on CD/TPGS ratio (SI, Figure S4A). Indeed, at 3% DIMEB the solution is slightly turbid and stable over time, while it is transparent at 5%.

The kinetics of micellisation from scattering techniques has been recently reviewed by Lund *et al*, with a focus on block copolymer micelles[48]. For low molecular weight micelles, the process can be well described by Aniansson and Wall theory[49], developed for near-equilibrium relaxation kinetics in terms of the rate constants of incorporation of a unimer into a micelle and its dissociation. For example, studies by gradient NMR of Pluronic P85[50] (which has a similar aggregation number than TPGS) indicated a fast exchange between free and micellized P85 molecules, with a lifetime of the surfactant in the micelles between 1 μs and 3 ms. T-jump studies on the micellar kinetics of Pluronics F127, F88 and P123 revealed a single relaxation time in the millisecond range, which was attributed to the exchange process[51]. Zana *et al.* investigated Pluronic L64 by ultrasonic absorption and T-jump methods, concluding that the exchange process takes place on the microsecond timescale and that there is essentially no energy barrier to the incorporation of a free unimer into the surfactant micelles upon collision, as the PPO block does not differ much in nature from the PEO shell that surrounds the Pluronic core[52]. The behavior of TPGS should not be very different from that of Pluronics, as the unimer has to cross a highly hydrated corona, to incorporate or leave the micelles. Regarding the kinetics of inclusion complex formation with CDs, the reaction can take place over a wide span of timescales, depending on the guest, but for small guests it is usually of the order of microseconds. As an example, a study by ultrasonic relaxation on a homologue series of carboxylic acids showed that the rate constants for the inclusion of pentanoic acid into β-CD and its removal from the cavity were 7.3×10^8 $mol^{-1}\cdot dm^3\cdot s^{-1}$ and 0.89×10^7 s^{-1}, respectively, the geometrical fit of the guest molecule within the cavity being a key factor to control the reaction rate[53].

To gain some insight into the CD-triggered de-micellization process from TR-SANS, we propose here a simple model in which the overall scattering is split up between two contributions: one due to the large aggregates, considered as spherical,

with a sld equivalent to that of a micelle (calculated as 4.7×10^{-6} Å^{-2}, from the results shown in Table 1) and another one due to the TPGS-DIMEB complex, which is modelled as a small sphere of sld equivalent to one TPGS molecule and three DIMEB, at 8.4×10^{-7} Å^{-2} (this specific stoichiometry is justified further down). The system is therefore modelled as a binary mixture of hard-spheres, which includes a hard sphere interaction between all the particles[54]. Figure 6 shows some of the most relevant findings obtained with this model.

Consideration of these plots leads to several conclusions. First, the TPGS-DIMEB complex has a constant size ($R \approx 25$ Å) (Figure 6C) and volume fraction (Figure 6D), matching reasonably well the size obtained by DLS or SANS, and confirms that the complex is totally formed after ca. 100 ms. Second, the kinetic data reveal the presence of large aggregates, whose size and fraction evolve over time (Figure 6A and B). At 100 ms, their size (at 60 Å) is close to the size of micelles (Figure 6A), and their volume fraction (about 0.006, Figure 6B) has dropped considerably compared to a 1% TPGS solution (0.027, Table 1), but shows that micelles are still present in the early stages of the complexation. After a few seconds, the aggregates increase in size (reaching a maximum of ca. 180 Å after 10 s), while their volume fraction decreases (down to 0.002). While the precise composition (or structure) of these aggregates is unknown, they should comprise a mixture of TPGS and DIMEB. At sufficiently long times, these aggregates remain in solution (at least at 3%), while at higher DIMEB concentrations (5%), their volume contribution becomes negligible (SI, Figure S4B). Overall, the kinetics of micellar disruption by CD are extremely fast, with a near-instantaneous disappearance of the micelles and the formation of TPGS-CD complexes in less than 100 ms. TR-SANS also reveal that micellar rupture is accompanied, rather surprisingly, by the formation of large, indiscriminate aggregates (at this intermediate DIMEB concentration of 3%), whose size and volume fraction evolve over time, although their contribution by volume or mass remains rather small.

Topology of the TPGS-DIMEB complex

More details on the structure of the inclusion complex, i.e. its stoichiometry and the location of the CDs on the amphiphile, were obtained from NMR. The first question to address is whether the macrocycle is threaded through the surfactant

headgroup (PEO block) or the hydrophobic tail (tocopherol moiety); for this purpose, we have focused on protons from both molecules that may undergo changes in their positions. Signal assignation of the DIMEB protons has been reported elsewhere[33], while that of TPGS in DMSO was carried out with the aid of the corresponding 1D and COSY spectrum (SI, Figure S6).

Figure 7 presents the spectra obtained from TPGS/DIMEB mixtures at varying ratios, showing the aliphatic region of TPGS. Noticeable changes in the *d* and *e* protons of TPGS (directly bonded to the aromatic ring) occur with increasing DIMEB fraction, with an increase in the signals at 2.0 and 2.2 ppm, accompanied by a reduction and vanishing of signals at 1.8 and 1.9 ppm. The aliphatic zone between 1.0 and 1.5 ppm, corresponding to the resonances of CH_3(a) and CH_2(b), shows a broad overlap that is difficult to track, but new signals at 1.25 and 1.35 ppm appear, along with the concomitant reduction of the ones at 1.0 and 1.1. In contrast, the resonance at 3.64 ppm (data not shown), due to the EO residues, does not change, even at high concentrations of DIMEB. Protons H(3) and H(5) from DIMEB (which point towards the center of the cavity and are typically used to confirm the formation of an inclusion complex), are shifted upfield by about 0.1 ppm and become broader (SI, Figure S7), while a much smaller shift (of about 0.03), is detected in the external H(1) protons, which appear in a zone free of overlap (SI, Figure S7), unlike H(2) or H(4). All these observations confirm the formation of a TPGS-DIMEB inclusion complex, and indicate that DIMEB is localized on the tocopheryl moiety, and not on the PEO chain.

It is worth mentioning that signal splitting, rather than shifting, occurs with the surfactant protons, but not with those from the macrocycle. This behavior can be explained in terms of the two simultaneous equilibria that are taking place: complexation with CD, and TPGS micellization, both occurring on a different time-scale. The lack of new signals in the spectrum of DIMEB at low DIMEB/TPGS ratios implies that the reaction in which the CD is involved (complexation) occurs at a fast exchange rate, leading to a shift in the resonances (such as H(3) and H(5)), rather than the appearance of new ones. In contrast, TPGS micellization must occur at a slower exchange rate compared to the NMR timescale, as reflected in the splitting of *d* and *e* protons. This (relatively) slower kinetics of micellization compared to the exchange rate of the surfactant in and out of the cyclodextrin confirms the fast micelle disruption process observed by TR-SANS. At higher DIMEB/TPGS molar ratios, there are no longer micelles, but only complexed monomers, which show a different

spectrum compared to the surfactant alone in water (Figure 7). A similar behavior has been observed in gemini cationic surfactants with different spacer groups[55], and most recently in a ruthenium metallosurfactant[56].

The precise location of the macrocycle was further ascertained from 2D-ROESY spectroscopy, which provides information of the interactions between protons that are spatially close, producing a NOE resonance (Figure 8). A clear cross peak between the cavity protons (H(3) and H(5)) with the CH_3(a) of TPGS is detected (circle 1, Figure 8), which confirms that DIMEB is threading the hydrophobic part of TPGS. A NOE resonance is also observed between the internal protons of the CD and the CH_2(b) of TPGS (circle 2, Figure 8). This cross peak is less intense than the former, as methylene groups are less bulky than CH_3, implying a larger distance between these protons and the cavity protons of DIMEB (the CH_3(a) can be distinguished from the CH_2(b) by their different areas in the 1D spectrum). In addition, an intense NOE between the CH_3(a) of TPGS and the protons at the primary rim of DIMEB, Me(6), is also detected (circle 3, Figure 8). These CD protons (21 in total) are at the narrower rim of the cavity, spatially close to the protuberant methyl groups of the tocopherol moiety, contributing to the relatively high intensity of this cross-peak. It is worth noting that, although *d* and *e* protons (from the benzene ring of TPGS) undergo an important shift (Figure 8), along with corresponding changes in the fluorescence spectra in the presence of DIMEB (Figure 4), no cross-peak in the ROESY spectrum appears between these and the cavity protons (Figure 8). A possible explanation for this is that CH_3(*d*) and CH_3(*e*) are acting as a steric barrier that prevents further "hopping" of the CD beyond the benzene. A shallow inclusion of the aromatic ring, with a subsequent change in its micropolarity (when going from the micellar state to the complexed monomer) may account for the observed changes in the fluorescence spectra.

The precise stoichiometry of the complex can also be obtained from NMR, using a Job's plot. The signals from selected protons of DIMEB are plotted as a function of CD mole fraction, χ_{DIMEB} (Figure 9). The curves all show a maximum which varies between 0.67 and 0.75, corresponding to a 2:1 or a 3:1 stoichiometry (CD:TPGS). A multivariable fit to H(3), H(5) and H(1) protons to a 2:1 consecutive equilibrium was attempted, but did not yield reliable values of K_1 and K_2, thus pointing to a 3:1 complex. A further estimation of the stoichiometry can also be

obtained by following the procedure based on the Hill's equation, which also provides information on the cooperative nature of the complexation, and was recently applied to pseudopolyrotaxanes of poloxamines and DIMEB[30]. In brief, it consists in finding the concentration of free CD from NMR data, assuming that the chemical shift of a CD proton in the complex does not depend sensibly on the degree of threading, as the magnetic environments must be similar. Under this assumption, the fraction of binding sites of TPGS occupied by CD, θ, can be expressed as:

$$\theta = \frac{[CD]^h}{[CD]^h + K_i^h} \qquad \text{Eq.8}$$

where [*CD*] is the concentration of free host, K_i an average microscopic dissociation constant, and *h* is the Hill coefficient, describing the cooperativity of the binding. [*CD*] and θ were estimated from the protons of DIMEB whose resonances undergo the largest shifts and can thus be unambiguously tracked (H(1), H(3), H(5) and Me(6)), by averaging both variables calculated for each dataset (SI, Figure S8). Following this procedure, a value of 1.9 ± 0.5 was obtained for *h*, indicating a rather positively cooperative process, in which the entrance of a macrocycle is favoured once a CD is already complexed. In addition, the saturation is reached at exactly $n = 3$, which confirms the 3:1 stoichiometry. The fitted average microscopic dissociation constant obtained is $K_i = (1.3 \pm 0.2) \times 10^{-4}$ mol·L^{-1}, equivalent to a binding constant per equilibrium log K_b = 3.9, a value typical of 1:1 complexes of βCDs with bulky aliphatic guests. For comparison, for the complex of poloxamine T904 with DIMEB, log K_b is lower, at 2.38[30], a consequence of propylene oxide being less bulky and hydrophobic than the hydrocarbon chain of tocopherol. It is worth noting that the Hill's equation only has a semi-empirical character, and the binding constant reported above is not the actual intrinsic constant per site. In the case of equivalent binding sites, Hill's equation reduces to the Langmuir one:

$$\theta = \frac{[CD]^n}{[CD]^n + K^n} \qquad \text{Eq. 9}$$

where *n* is the number of sites (3 in this system), and *K* the global thermodynamic constant for the dissociation reaction, from which the actual intrinsic constant can be obtained by statistical considerations. By imposing the condition that the sites are

equivalent (h = 3 in Hill's equation) we obtain a very similar K value of (1.2 ± 0.1)×10^{-4} mol·L^{-1}, suggesting that the cooperative effect is not very remarkable in this system. We refer the reader to reference [57] for a deeper understanding of this topic, which is sometimes overlooked in the scientific literature.

SUMMARY AND CONCLUSIONS

We have reported in this work a comprehensive structural investigation on the aggregation process of TPGS-1000 micelles, using scattering and spectroscopic methods. TPGS micelles form gradually, rather than showing the sharp aggregation onset typical of smaller surfactants. The micelles display a core-shell architecture with a core of ~ 38 Å and a largely hydrated PEO shell of ~ 28 Å. The micelles were remarkably insensitive to both concentration and temperature, a critical advantage in the application of this surfactant as a drug carrier. The impact that different cyclodextrins (CDs) have on the self-assembly of TPGS was studied, and show that not only the nature of the substituents, but also the substitution pattern (random, or regular) are critical in determining the outcome. Native CDs consistently lead to the precipitation of a polypseudorotaxane, resulting from the threading of the PEG and/or the tocopheryl moiety of TPGS by the macrocycle, as has been reported for PEO or PEO-based amphiphilic block-copolymers. DIMEB, a βCD which is regularly dimethylated in positions 2 and 6, strongly disrupts the aggregation process, as consistently observed throughout our work with other amphiphilic macromolecules, while the thrice-methylated equivalent (TRIMEB) has no detectable effect, and a randomly methylated βCD (RAMEB) induces the formation of large, indiscriminate aggregates. Other randomly substituted CDs, like HPBCD or HEBCD, do not seem to modify the aggregation behavior of TPGS, which may be of interest for the combined use of this surfactant and CDs including a drug in the cavity, for example.

Kinetic pathways of were explored by time-resolved SANS for the surfactant and DIMEB, revealing extremely fast kinetics of micelle disruption (< 100 ms, the limit of detection of the technique) and the formation of large aggregates, whose size and volume fraction evolve over time, alongside the TPGS-DIMEB complex which forms instantaneously. These large aggregates are not present at higher DIMEB/TPGS ratios. 1H and ROESY NMR experiments demonstrate that DIMEB solubilizes TPGS by the incorporation of up to three macrocycles on the tocopheryl part of the molecule in a

rather cooperative process, in which the incorporation of a CD favors the subsequent threading of the aliphatic chain.

Overall, the systematic study presented here provides detailed structural and mechanistic information on TPGS associative behavior, kinetic pathways and their modulation by cyclodextrins. This detailed understanding should help provide a solid basis for the design of multi-component drug delivery systems based on these two FDA-approved, attractive pharmaceutical excipients.

ACKNOWLEDGMENTS

The authors thank ISIS and the ILL for the provision of beam time, and in particular Richard Heenan (Rutherford Appleton Laboratory) for assistance with the SANS experiments. Prof. G. Tardajos (UCM) and R. Serra (UN) are acknowledged for their help with the NMR and TR-SANS measurements. Financial support from project MAT2014-59116-C2-2-R of the Spanish MINECO and the Asociación de Amigos of the University of Navarra for the doctoral grant of J.P. is acknowledged.

SUPPORTING INFORMATION

Structure of the repeating units of the cyclodextrin derivatives; absorption spectra and Beer-Lambert plot for TPGS; diffusion coefficients (DLS) of TPGS as a function of concentration and temperature; intensity size distribution (DLS) of mixtures of TPGS with αCD in water; intensity and volume size distributions (DLS) for TPGS and mixtures with DIMEB in D_2O; fluorescence decays and corresponding fits of TPGS in the presence of DIMEB; NMR spectra of TPGS and mixtures with DIMEB; Hill's plot for the system TPGS + DIMEB; table of fluorescence lifetimes of TPGS as a function of concentration.

REFERENCES

(1) Sadoqi, M.; Lau-Cam, C.; Wu, S. H. Investigation of the Micellar Properties of the Tocopheryl Polyethylene Glycol Succinate Surfactants TPGS 400 and TPGS 1000 by Steady State Fluorometry. *J. Colloid Interface Sci.* **2009**, *333* (2), 585–589.

(2) Zhang, Z.; Tan, S.; Feng, S.-S. Vitamin E TPGS as a Molecular Biomaterial for Drug Delivery. *Biomaterials* **2012**, *33* (19), 4889–4906.

(3) Collnot, E.-M.; Baldes, C.; Wempe, M. F.; Hyatt, J.; Navarro, L.; Edgar, K. J.; Schaefer, U. F.; Lehr, C.-M. Influence of Vitamin E TPGS Poly(ethylene Glycol) Chain Length on Apical Efflux Transporters in Caco-2 Cell

Monolayers. *J. Control. Release* **2006**, *111* (1–2), 35–40.

(4) Guo, Y.; Luo, J.; Tan, S.; Otieno, B. O.; Zhang, Z. The Applications of Vitamin E TPGS in Drug Delivery. *Eur. J. Pharm. Sci.* **2013**, *49* (2), 175–186.

(5) Khare, V.; Sakarchi, W. A.; Gupta, P. N.; Curtis, A. D. M.; Hoskins, C. Synthesis and Characterization of TPGS–gemcitabine Prodrug Micelles for Pancreatic Cancer Therapy. *RSC Adv.* **2016**, *6* (65), 60126–60137.

(6) Moretton, M. A.; Taira, C.; Flor, S.; Bernabeu, E.; Lucangioli, S.; Höcht, C.; Chiappetta, D. A. Novel Nelfinavir Mesylate Loaded D-α-Tocopheryl Polyethylene Glycol 1000 Succinate Micelles for Enhanced Pediatric Anti HIV Therapy: In Vitro Characterization and in Vivo Evaluation. *Colloids Surfaces B Biointerfaces* **2014**, *123*, 302–310.

(7) Ha, E.-S.; Baek, I.; Kim, M.-S. Preparation and Characterization of TPGS-Colloidal Silica Microparticles for Enhancement of Solubility and Oral Bioavailability of Lercanidipine Hydrochloride. *Bull. Korean Chem. Soc.* **2016**, *37* (5), 660–666.

(8) Bao, X.; Gao, M.; Xu, H.; Liu, K.-X.; Zhang, C.-H.; Jiang, N.; Chu, Q.-C.; Guan, X.; Tian, Y. A Novel Oleanolic Acid-Loaded PLGA-TPGS Nanoparticle for Liver Cancer Treatment. *Drug Dev. Ind. Pharm.* **2015**, *41* (7), 1193–1203.

(9) Ishak, R. A. H.; Osman, R. Lecithin/TPGS-Based Spray-Dried Self-Microemulsifying Drug Delivery Systems: In Vitro Pulmonary Deposition and Cytotoxicity. *Int. J. Pharm.* **2015**, *485* (1–2), 249–260.

(10) Kutty, R. V.; Chia, S. L.; Setyawati, M. I.; Muthu, M. S.; Feng, S.-S.; Leong, D. T. In Vivo and Ex Vivo Proofs of Concept That Cetuximab Conjugated Vitamin E TPGS Micelles Increases Efficacy of Delivered Docetaxel against Triple Negative Breast Cancer. *Biomaterials* **2015**, *63*, 58–69.

(11) Mi, Y.; Zhao, J.; Feng, S.-S. Vitamin E TPGS Prodrug Micelles for Hydrophilic Drug Delivery with Neuroprotective Effects. *Int. J. Pharm.* **2012**, *438* (1–2), 98–106.

(12) Duhem, N.; Danhier, F.; Preat, V. Vitamin E-Based Nanomedicines for Anti-Cancer Drug Delivery. *J. Control. Release* **2014**, *182*, 33–44.

(13) Mei, L.; Zhang, Z.; Zhao, L.; Huang, L.; Yang, X.-L.; Tang, J.; Feng, S.-S. Pharmaceutical Nanotechnology for Oral Delivery of Anticancer Drugs. *Adv. Drug Deliv. Rev.* **2013**, *65* (6), 880–890.

(14) Vandecruys, R.; Peeters, J.; Verreck, G.; Brewster, M. E. Use of a Screening

Method to Determine Excipients Which Optimize the Extent and Stability of Supersaturated Drug Solutions and Application of This System to Solid Formulation Design. *Int. J. Pharm.* **2007**, *342* (1–2), 168–175.

(15) Singh, R. P.; Sharma, G.; Sonali; Singh, S.; Patne, S. C. U.; Pandey, B. L.; Koch, B.; Muthu, M. S. Effects of Transferrin Conjugated Multi-Walled Carbon Nanotubes in Lung Cancer Delivery. *Mater. Sci. Eng. C* **2016**, *67*, 313–325.

(16) Szente, L.; Szejtli, J. Cyclodextrins as Food Ingredients. *Trends in Food Science & Technology*. **2004**, 15 (3), 137-142.

(17) Davis, M. E.; Brewster, M. E. Cyclodextrin-Based Pharmaceutics: Past, Present and Future. *Nat. Rev. Drug Discov.* **2004**, *3* (12), 1023–1035.

(18) Uekama, K. Design and Evaluation of Cyclodextrin-Based Drug Formulation. *Chem. Pharm. Bull. (Tokyo).* **2004**, *52* (8), 900–915.

(19) Otero-Espinar, F. J.; Blanco-Mendez, J. Natural & Synthetically-Modified Cyclodextrins and Polymers in Drug Delivery Systems. *Curr. Top. Med. Chem.* **2014**, *14* (4), 463–464.

(20) Jambhekar, S. S.; Breen, P. Cyclodextrins in Pharmaceutical Formulations I: Structure and Physicochemical Properties, Formation of Complexes, and Types of Complex. *Drug Discov. Today* **2016**, *21* (2), 356–362.

(21) Simoes, S. M. N.; Rey-Rico, A.; Concheiro, A.; Alvarez-Lorenzo, C. Supramolecular Cyclodextrin-Based Drug Nanocarriers. *Chem. Commun.* **2015**, *51* (29), 6275–6289.

(22) Li, J.; Loh, X. Cyclodextrin-Based Supramolecular Architectures: Syntheses, Structures, and Applications for Drug and Gene Delivery. *Adv. Drug Deliv. Rev.* **2008**, *60* (9), 1000–1017.

(23) Zhang, J.; Ma, P. X. Cyclodextrin-Based Supramolecular Systems for Drug Delivery: Recent Progress and Future Perspective. *Adv. Drug Deliv. Rev.* **2013**, *65* (9), 1215–1233.

(24) Garcia-Rio, L.; Otero-Espinar, F. J.; Luzardo-Alvarez, A.; Blanco-Mendez, J. Cyclodextrin Based Rotaxanes, Polyrotaxanes and Polypseudorotaxanes and Their Biomedical Applications. *Curr. Top. Med. Chem.* **2014**, *14* (4), 478–493.

(25) Wenz, G.; Han, B.-H.; Müller, A. Cyclodextrin Rotaxanes and Polyrotaxanes. *Chem. Rev.* **2006**, *106* (3), 782–817.

(26) Nelson, A.; Stoddart, J. F. Dynamic Multivalent Lactosides Displayed on

Cyclodextrin Beads Dangling from Polymer Strings. *Org. Lett.* **2003**, *5* (21), 3783–3786.

(27) Nelson, A.; Belitsky, J. M.; Vidal, S.; Joiner, C. S.; Baum, L. G.; Stoddart, J. F. A Self-Assembled Multivalent Pseudopolyrotaxane for Binding Galectin-1. *J. Am. Chem. Soc.* **2004**, *126* (38), 11914–11922.

(28) Mondjinou, Y. A.; McCauliff, L. A.; Kulkarni, A.; Paul, L.; Hyun, S.-H.; Zhang, Z.; Wu, Z.; Wirth, M.; Storch, J.; Thompson, D. H. Synthesis of 2-Hydroxypropyl-β-cyclodextrin/Pluronic-Based Polyrotaxanes via Heterogeneous Reaction as Potential Niemann-Pick Type C Therapeutics. *Biomacromolecules* **2013**, *14* (12), 4189–4197.

(29) Simoes, S.; Veiga, F.; Torres-Labandeira, J.; Ribeiro, A.; Concheiro, A.; Alvarez-Lorenzo, C. Syringeable Self-Assembled Cyclodextrin Gels for Drug Delivery. *Curr. Top. Med. Chem.* **2014**, *14* (4), 494–509.

(30) González-Gaitano, G.; Müller, C.; Radulescu, A.; Dreiss, C. A. Modulating the Self-Assembly of Amphiphilic X-Shaped Block Copolymers with Cyclodextrins: Structure and Mechanisms. *Langmuir* **2015**, *31* (14), 4096–4105.

(31) González-Gaitano, G.; da Silva, M. A.; Radulescu, A.; Dreiss, C. A. Selective Tuning of the Self-Assembly and Gelation of a Hydrophilic Poloxamine by Cyclodextrins. *Langmuir* **2015**, *31* (20), 5645–5655.

(32) González-Gaitano, G.; Isasi, J. R.; Vélaz, I.; Zornoza, A. Drug Carrier Systems Based On Cyclodextrin Supramolecular Assemblies And Polymers: Present And Perspectives. *Curr. Pharm. Des.* **2017**, *23* (3),411-432.

(33) Castiglione, F.; Valero, M.; Dreiss, C. A.; Mele, A. Selective Interaction of 2,6-Di-O-Methyl-β-Cyclodextrin and Pluronic F127 Micelles Leading to Micellar Rupture: A Nuclear Magnetic Resonance Study. *J. Phys. Chem. B* **2011**, *115* (29), 9005–9013.

(34) Http://www.sasview.org/. Developed by the DANSE Project under NSF Award DMR-0520547.

(35) Grillo, I. Applications of Stopped-Flow in SAXS and SANS. *Curr. Opin. Colloid Interface Sci.* **2009**, *14* (6), 402–408.

(36) Http://www.ill.fr/data_treat/lamp/lamp.html. LAMP (Large Array Manipulation Program), developed by Institut Laue-Langevin.

(37) Dreiss, C. A.; González-Gaitano, G.; Grillo, I.; Serra-Gómez, R. Unravelling the Mechanisms of Complexation between Tetronics and Cyclodextrins.

Institute Laue-Langevin (ILL) doi:10.5291/ILL-DATA.9-12-401.

(38) Bisby, R.; Ahmed, S. Transverse Distribution of α-Tocopherol in Bilayer Membranes Studied by Fluorescence Quenching. *Free Radic. Biol. Med.* **1989**, *6* (3), 231–239.

(39) Serra-Gómez, R.; Dreiss, C. A.; González-Benito, J.; González-Gaitano, G. Structure and Rheology of Poloxamine T1107 and Its Nanocomposite Hydrogels with Cyclodextrin-Modified Barium Titanate Nanoparticles. *Langmuir* **2016**, *32* (25), 6398–6408.

(40) González-Gaitano, G.; Rodríguez, P.; Isasi, J. R.; Fuentes, M.; Tardajos, G.; Sánchez, M. The Aggregation of Cyclodextrins as Studied by Photon Correlation Spectroscopy. *J. Incl. Phenom. Macrocycl. Chem.* **2002**, *44* (1–4), 101–105.

(41) Dreiss, C. A.; Cosgrove, T.; Newby, F. N.; Sabadini, E. Formation of a Supramolecular Gel between α-Cyclodextrin and Free and Adsorbed PEO on the Surface of Colloidal Silica: Effect of Temperature, Solvent, and Particle Size. *Langmuir* **2004**, *20* (21), 9124–9129.

(42) Harada, A.; Kamachi, M. Complex Formation between Cyclodextrin and Poly(propylene Glycol). *J. Chem. Soc. Chem. Commun.* **1990**, No. 19, 1322.

(43) Dreiss, C. A.; Nwabunwanne, E.; Liu, R.; Brooks, N. J. Assembling and de-Assembling Micelles: Competitive Interactions of Cyclodextrins and Drugs with Pluronics. *Soft Matter* **2009**, *5* (9), 1888–1896.

(44) Valero, M.; Dreiss, C. A. Growth, Shrinking, and Breaking of Pluronic Micelles in the Presence of Drugs And/or β-Cyclodextrin, a Study by Small-Angle Neutron Scattering and Fluorescence Spectroscopy. *Langmuir* **2010**, *26* (13), 10561–10571.

(45) Valero, M.; Castiglione, F.; Mele, A.; da Silva, M. A.; Grillo, I.; González-Gaitano, G.; Dreiss, C. A. Competitive and Synergistic Interactions between Polymer Micelles, Drugs, and Cyclodextrins: The Importance of Drug Solubilization Locus. *Langmuir* **2016**, *32* (49), 13174–13186.

(46) da Silva, M. A.; Weinzaepfel, E.; Afifi, H.; Eriksson, J.; Grillo, I.; Valero, M.; Dreiss, C. A. Tuning the Viscoelasticity of Nonionic Wormlike Micelles with β-Cyclodextrin Derivatives: A Highly Discriminative Process. *Langmuir* **2013**, *29* (25), 7697–7708.

(47) Bleta, R.; Machut, C.; Léger, B.; Monflier, É.; Ponchel, A. Coassembly of

Block Copolymer and Randomly Methylated β-Cyclodextrin: From Swollen Micelles to Mesoporous Alumina with Tunable Pore Size. *Macromolecules* **2013**, *46* (14), 5672–5683.

(48) Lund, R.; Willner, L.; Richter, D. Kinetics of Block Copolymer Micelles Studied by Small-Angle Scattering Methods. In *Advances in Polymer Science*; 2013; pp 51–158.

(49) Aniansson, E. A. G.; Wall, S. N. Kinetics of Step-Wise Micelle Association. Correction and Improvement. *J. Phys. Chem.* **1975**, *79* (8), 857–858.

(50) Fleischer, G. Micellization in Aqueous Solution of a Poly(ethylene Oxide)/poly(propylene Oxide)/poly(ethylene Oxide) Triblock Copolymer Investigated with Pulsed Field Gradient NMR. *J. Phys. Chem.* **1993**, *97* (2), 517–521.

(51) Hecht, E.; Hoffmann, H. Kinetic and Calorimetric Investigations on Micelle Formation of Block-Copolymers of the Poloxamer Type. *Colloids Surfaces A Physicochem. Eng. Asp.* **1995**, *96* (1–2), 181–197.

(52) Michels, B.; Waton, G.; Zana, R. Dynamics of Micelles of Poly(ethylene oxide)−Poly(propylene oxide)−Poly(ethylene Oxide) Block Copolymers in Aqueous Solutions. *Langmuir* **1997**, *13* (12), 3111–3118.

(53) Nishikawa, S.; Kondo, M. Kinetic Study for the Inclusion Complex of Carboxylic Acids with Cyclodextrin by the Ultrasonic Relaxation Method. *J. Phys. Chem. B* **2006**, *110* (51), 26143–26147.

(54) Ashcroft, N. W.; Langreth, D. C. Structure of Binary Liquid Mixtures. I. *Phys. Rev.* **1967**, *156* (3), 685–692.

(55) Groth, C.; Nydén, M.; Holmberg, K.; Kanicky, J. R.; Shah, D. O. Kinetics of the Self-Assembly of Gemini Surfactants. *J. Surfactants Deterg.* **2004**, *7* (3), 247–255.

(56) Iza, N.; Guerrero-Martínez, A.; Tardajos, G.; Ortiz, M. J.; Palao, E.; Montoro, T.; Radulescu, A.; Dreiss, C. A.; González-Gaitano, G. Using Inclusion Complexes with Cyclodextrins To Explore the Aggregation Behavior of a Ruthenium Metallosurfactant. *Langmuir* **2015**, *31* (9), 2677–2688.

(57) Weiss, J. N. The Hill Equation Revisited: Uses and Misuses. *FASEB J.* **1997**, *11* (11), 835–841.

FIGURES

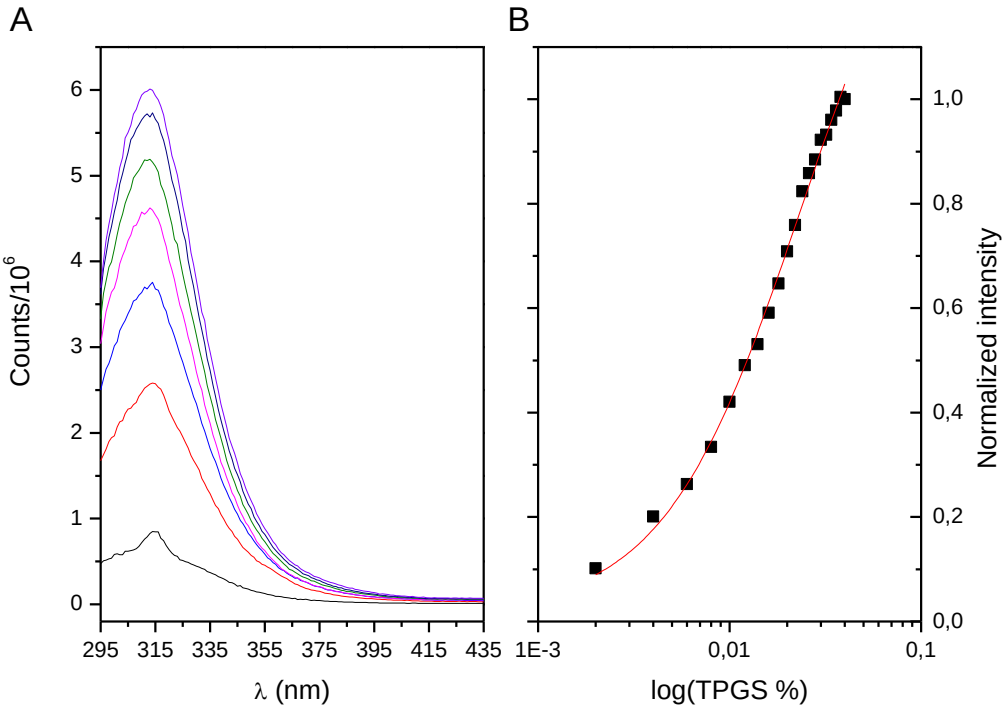

Figure 1. a) Fluorescence emission spectra of TPGS up to 0.04%; b) Normalized intensity at λ_{max}.

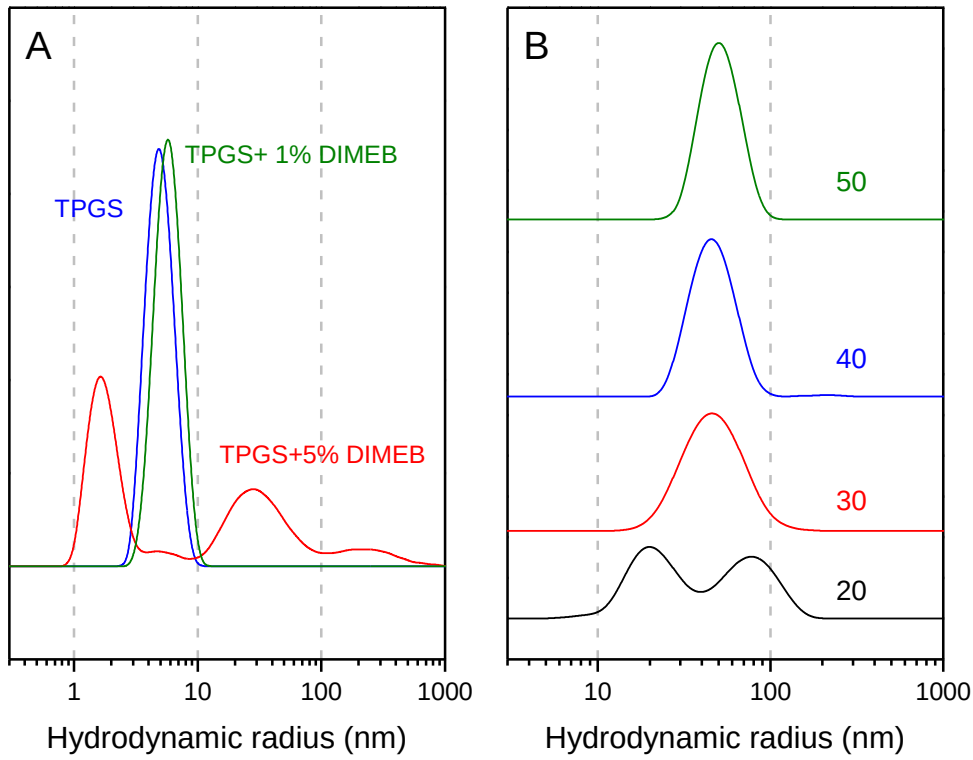

Figure 2. A. Intensity size distribution obtained by DLS at 20ºC from solutions of 1% TPGS alone (blue), and with the addition of 1% DIMEB (green) or 5% DIMEB (red); B. Intensity size distribution from a 1%TPGS solution with 5% RAMEB as a function of temperature.

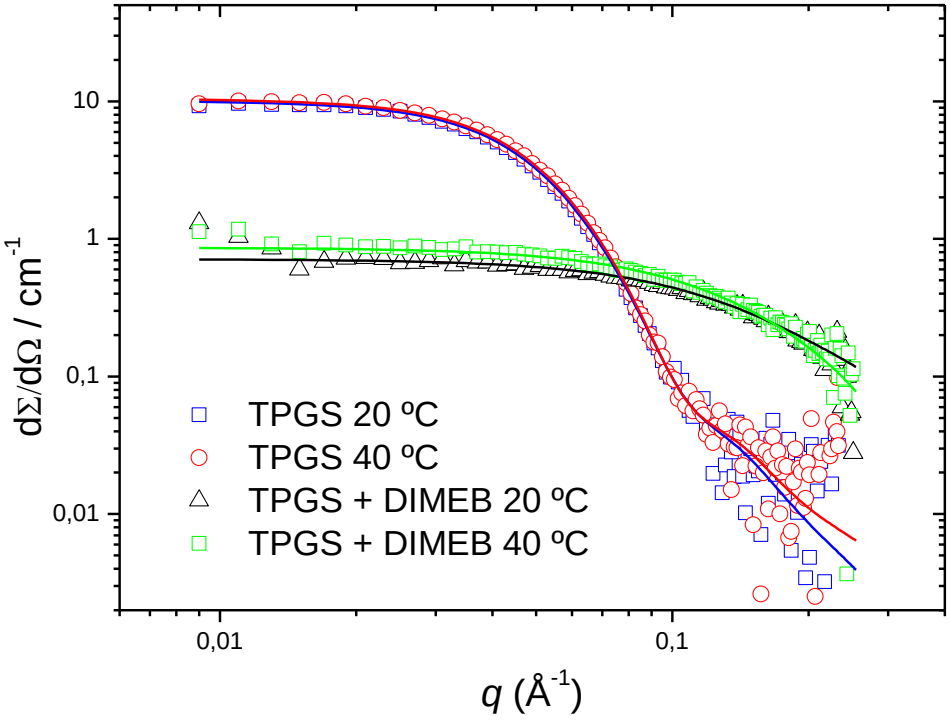

Figure 3. SANS from 1% TPGS in D_2O, alone and with 5% added DIMEB, at 20ºC and 40ºC.

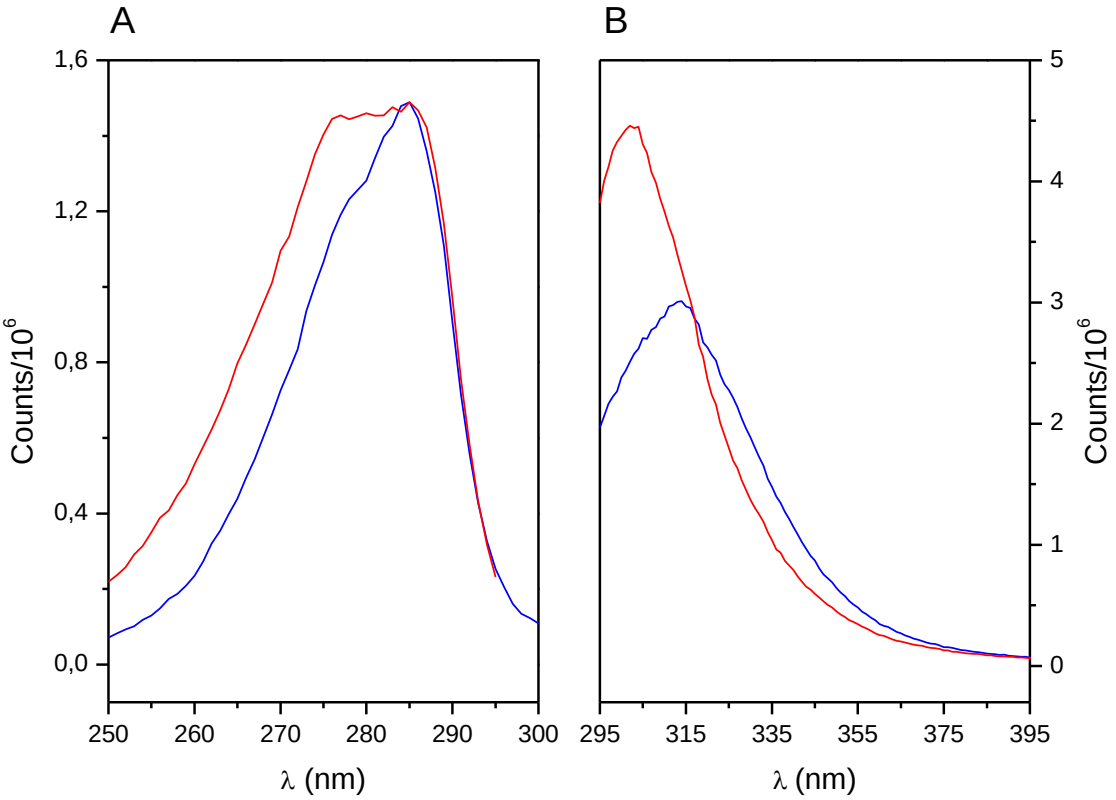

Figure 4. Excitation (A) and emission spectra (B) of 0.01% TPGS (blue) and with 3% DIMEB (red).

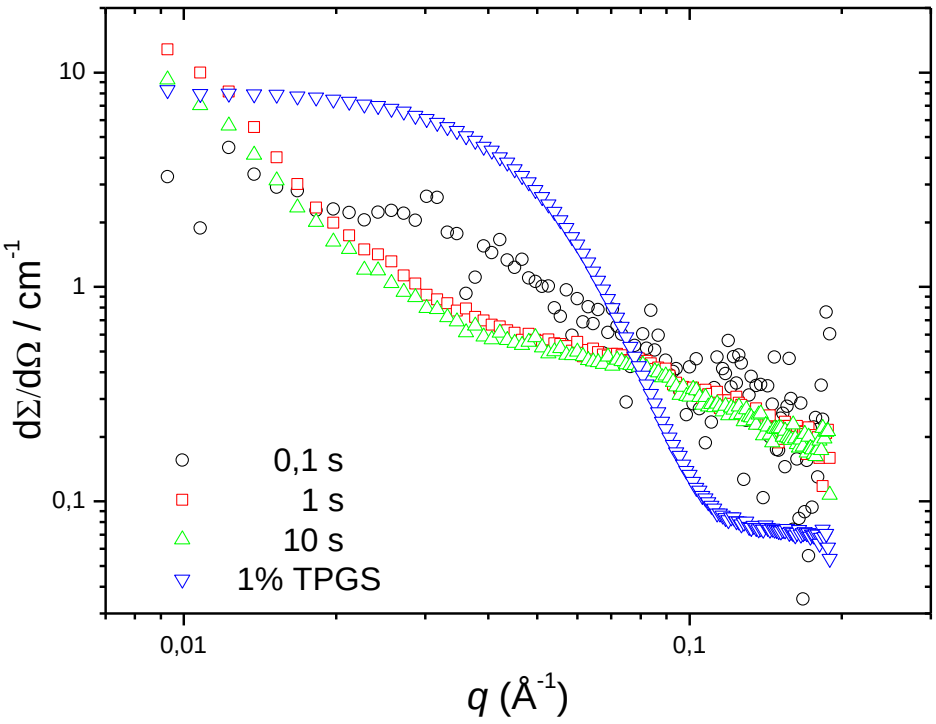

Figure 5. TR-SANS patterns for 1% TPGS with 3% DIMEB in D_2O at selected time points (40°C). For comparison purposes, the scattering from 1% TPGS alone is also shown.

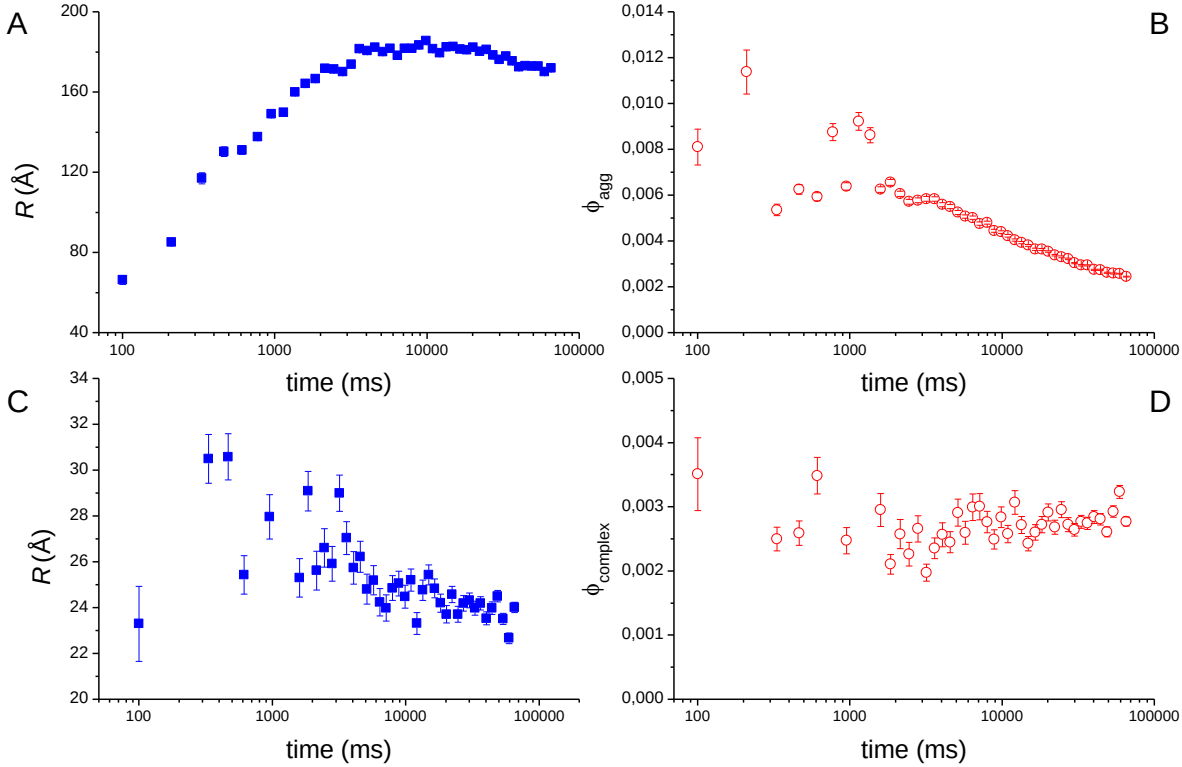

Figure 6. TR-SANS analysis of the kinetics of association between 1% TPGS and 3% DIMEB. The parameters shown result from modeling the scattering curves over a range of time points as a binary mixture of hard spheres (see text for details). A and B: Radius and volume fraction of the large aggregates; C and D: Radius and volume fraction of the TPGS-CD complex.

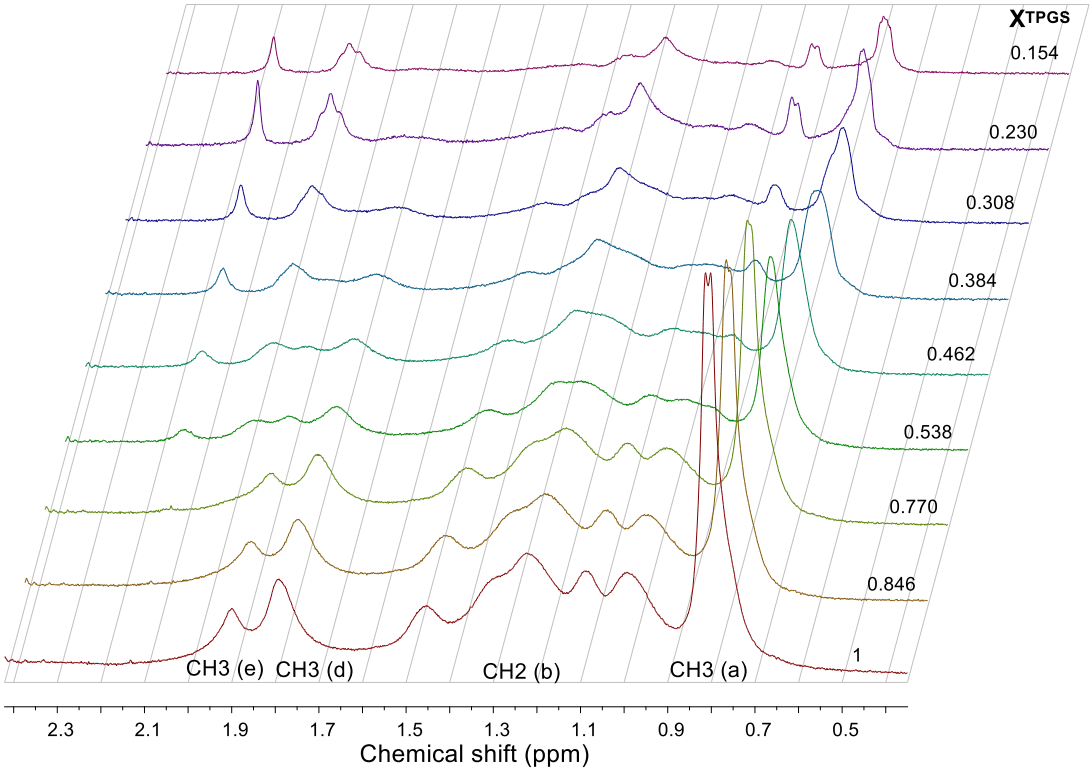

Figure 7. NMR spectra (aliphatic region) from mixtures of TPGS and DIMEB at varying ratios, expressed as TPGS mole fraction.

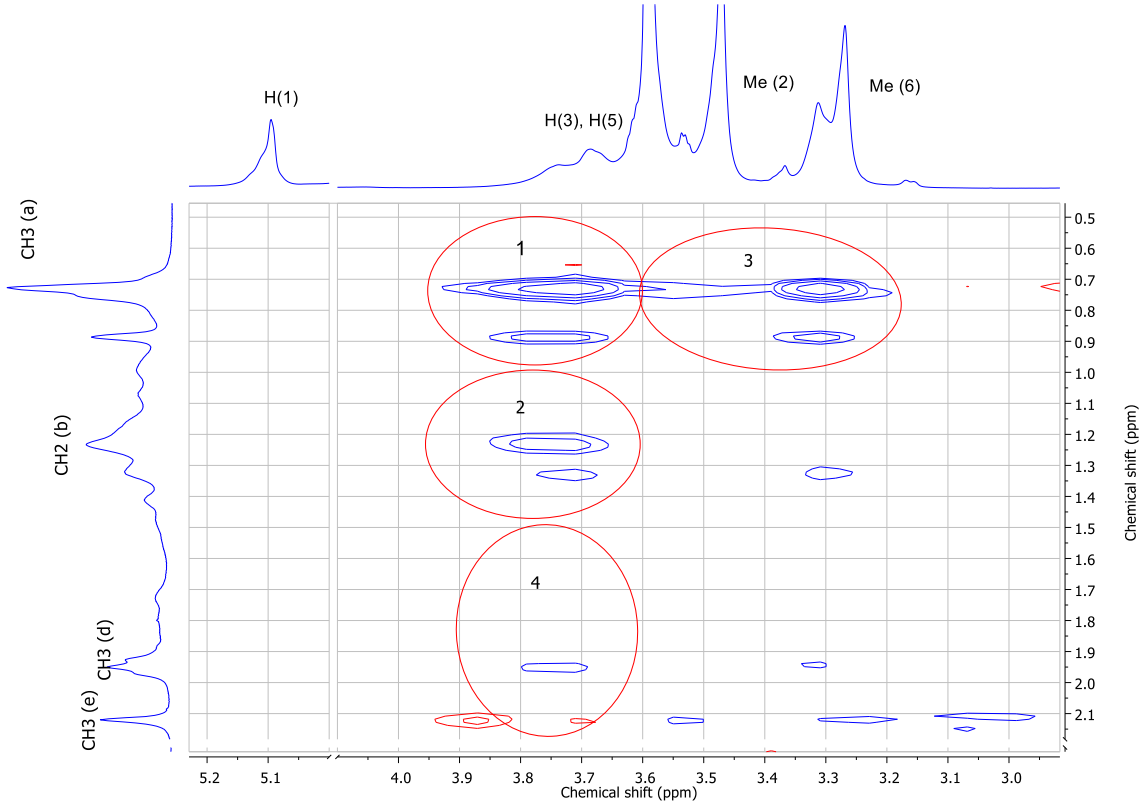

Figure 8. 2D-ROESY spectrum of 1% TPGS solution with 2% DIMEB in D_2O (χ_{DIMEB} = 0.69).

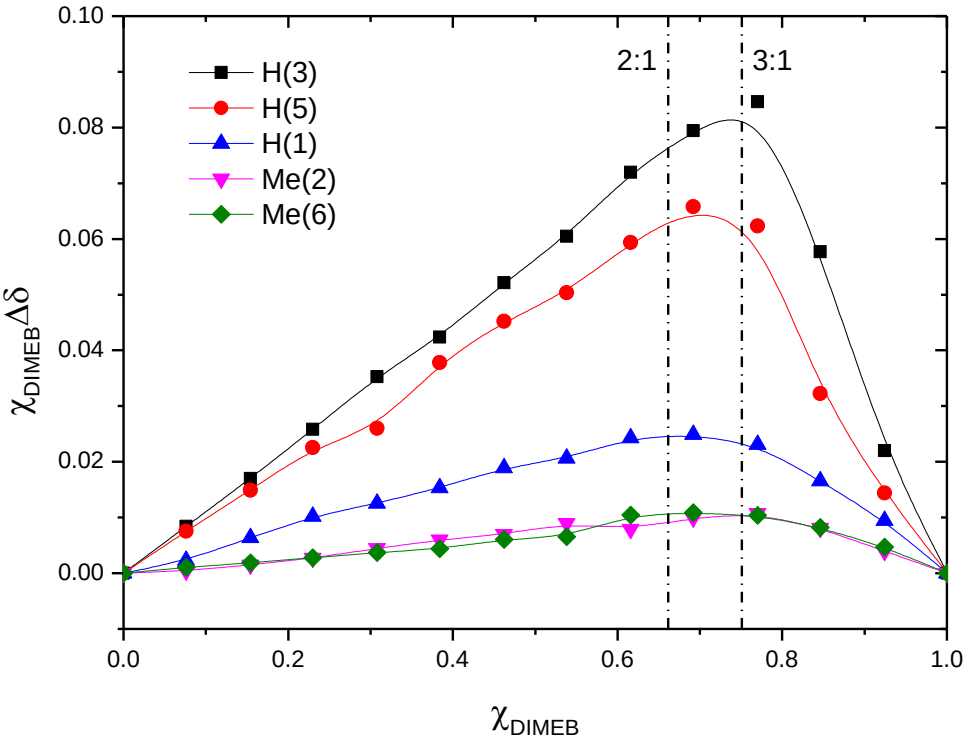

Figure 9. Job's plot for the complex between TPGS and DIMEB for selected protons of the cyclodextrin ($\Delta\delta$ is the difference in the chemical shift with respect to DIMEB alone). Vertical lines indicate the stoichiometry.

GRAPHICAL ABSTRACT